Engineering Structures 260 (2022) 114235

Contents lists available at ScienceDirect

Engineering Structures

journal homepage: www.elsevier.com/locate/engstruct

Cyclic behavior and design methodology of exposed base plates with extended anchor bolts

Pablo Torres-Rodas [a], Miguel Medalla [b], Farzin Zareian [c], Diego Lopez-Garcia [b,d,*]

[a] Universidad San Francisco de Quito USFQ, Colegio de Ciencias e Ingenierías, Campus Cumbayá, Quito 170901, Ecuador
[b] Department of Structural & Geotechnical Engineering, Pontificia Universidad Catolica de Chile, Chile
[c] Department of Civil & Environmental Engineering, University of California at Irvine, USA
[d] Research Center for Integrated Disaster Risk Management (CIGIDEN) ANID FONDAP 15110017, Chile

ARTICLE INFO

Keywords:
Column base connection
Exposed base plate
Extended anchor bolts

ABSTRACT

This paper investigates the behavior of a ductile detail of exposed base plates. This detail consists of a base plate anchored to the concrete foundation through bolts extended to a steel chair configuration. The intention is to concentrate plastic strains mainly in the extended region of the anchor bolts, forcing the other connection components to remain elastic. The scientific background of this research consists of a series of sophisticated nonlinear finite element models subjected to a cyclic load protocol in the presence of an axial compressive force. The models were validated against an experimental test reported in the literature. Forces within the connection components, stresses, strain distributions, and deformation modes were examined. A total of sixteen three-dimensional nonlinear models were created using the ABAQUS simulation platform. The models were separated into two groups: the first consists of models with dimensions similar to the specimens tested in recent experimental programs reported in the past, while the second group simulates connections representative of mid-rise industrial frames. Building on the insights gained from the simulations of the first group, a methodology is proposed to design these column base connections. This suggested methodology is validated with the second group of simulations. Results indicate that the studied configuration detail presents some advantages compared with the traditional detail presented in Design Guide 1. For instance, plastic strains are developed almost exclusively in the anchor rods, and no damage is expected at the remaining components. Another essential characteristic is the exposed stretch length, with which it is possible to achieve a target design rotation without significant strain concentrations in the anchor rods. This characteristic facilitates post-earthquake inspections and repairs, and damage is virtually eliminated in the first story.

1. Introduction

Column base connections (CBCs) are among the most critical components of Steel Moment Frames (SMFs); their behavior profoundly influences the overall performance of SMFs [1–4]. Early investigations on CBCs (e.g., [5–7]) alongside remarkable experimental programs on large-scale specimens (e.g., [8–12]) have provided insight into their behavior and failure modes. These tests led to the development of prominent analytical models to characterize the strength of CBCs (e.g., [13]). In the context of the US engineering practice, the Steel Design Guide 1 (DG1) [14] details the methodology to design exposed base plates (EBPs), the most common type of CBC. Together with the Seismic Design Manual [15], DG1 provides the basis for the modern design of EBPs. Subsequent studies conducted on this topic focused on refinements of the strength method presented in DG1 (e.g., [8–10]) and on methods to evaluate the base rotation flexibility and its impact on the overall seismic response of SMFs. For instance, Kanvinde et al. [16] proposed a practical method to estimate the base rotation flexibility by aggregating the deformations within the components of the CBC. Zareian and Kanvinde [1] studied the impact of the base rotation flexibility on the response of SMFs. Modern studies have addressed issues related to the hysteretic characteristics of CBCs [17–18], and computational studies based on sophisticated Finite Element (FE) models (e.g., [9,19]) have explored internal forces and stress distributions within the components of CBCs.

Other studies have focused on ductile details for anchor bolts

* Corresponding author.
E-mail address: dlg@ing.puc.cl (D. Lopez-Garcia).

https://doi.org/10.1016/j.engstruct.2022.114235
Received 8 November 2021; Received in revised form 20 February 2022; Accepted 1 April 2022
Available online 20 April 2022

embedded in concrete. For instance, Trautner et al. [20] carried out more than 90 tension tests of all-thread and headed anchors to understand the relationships between anchor deformation capacity and stretch length and to estimate strength characteristics. Parks et al. [21] tested individual anchor bolts with different stretch lengths (four, six, and eight times the bar diameter) and with two types of steel chair assemblies (one designed for remaining elastic and the other to yield) to examine their performance under combined shear and tension loads. Interestingly, the anchor bolts with a stretch length of at least four bar diameters lead to a more ductile connection than a conventional anchor bolt. These results motivated Parks et al. [22] to study experimentally and with finite element simulations the connection of a dry storage cask to the foundation using stretch length anchor bolts. Results indicate that this connection poses substantial energy dissipation properties. On the other hand, experimental programs conducted by Saleem and Gutierrez [23] and Saleem and Hosoda [24] have focused on non-destructive tests to evaluate crack detection and the pull-out strength of anchor bolts embedded in concrete. Saleem and Hosoda [24] proposed a non-destructive test that used the Schmidt hammer rebound number to estimate the load-carrying capacity of embedded anchor bolts. In the context of steel construction, this test can allow contractors to identify improperly installed bolts with low pull-out strength.

A recent experimental program conducted by Trautner et al. [11–12] investigated the performance of EBPs designed to promote anchor bolt yielding, denoted here EBP-ABYs. The main parameters analyzed in that study were the type of anchor bolt (i.e., cast-in, adhesive, and undercut anchors), the setting method (i.e., leveling nut, shim stacks), and the stretch length. All experimental results presented desirable hysteretic characteristics, and the rotation capacity of EBP-ABYs was mainly influenced by the type of anchor bolt and the stretch length. An important observation from these experiments is that some characteristics of EBP-ABYs are different from those of the *standard* connections, which usually have different yield mechanisms [8]. Specifically, the experimental evidence shows that EBP-ABYs have zero residual rotations, which contrasts with what is observed in standard connections (e.g., [8]). This self-centering characteristic of EBP-ABYs is important because it is consistent with the global self-centering frame behavior. Besides, strength and stiffness deterioration in EBP-ABYs are observed only at large deformations (0.10 rad or more), whereas in connections dominated by base plate yielding deterioration is observed at smaller rotations, between 0.03 rad and 0.05 rad [8,11].

Field evidence supports the experimental results and observations presented by Trautner et al. [11] regarding the performance of EBP-ABYs. For example, CBCs with a well-defined stretch length performed exceptionally well after the 2010 Maule (Chile) earthquake [25], especially in steel tanks and industrial facilities where plastic strains in the frames were minimal. On the other hand, CBCs without a well-defined stretch length presented anchor bolt fracture and failure of the connection [25]. In part, this successful experience has motivated researchers to explore alternative criteria to detail base plates [11–12]. In fact, due to the excellent performance of this configuration (i.e., well-defined strength length) after earthquake events (e.g., 2010 Maule (Chile)), ACI 318–11 [26] added such configuration as an anchor design option (Appendix E). However, studies conducted to understand and quantify the behavior of CBCs detailed to promote yielding in the stretch length of the anchor bolts are relatively sparse.

Currently, the seismic design provisions AISC 341–16 [27] indicate that the required strength of CBCs is the lesser of $1.1R_yF_yZ_x$ of the attached column (where R_yF_y is the expected yield stress and Z_x is the plastic modulus) and the amplified seismic load (i.e.,$\Omega_o = 3$). Studies conducted by Torres-Rodas et al. [28,29] indicate that the suggested strength capacity leads to an elastic behavior of the CBC and enforces yielding at the base of the first-story column. However, Lignos and Krawinkler [30] collected experimental data indicating that ductility in columns might be compromised due to local phenomena such as local buckling or lateral-torsional buckling, especially in the presence of axial loads. Thus, it appears that alternative design criteria intended to promote elastic behavior of the column and focus energy dissipation at another conveniently selected component of the CBC are promising and worthy of further research.

Motivated by the preceding discussion, this paper investigates the behavior of a ductile type of EBP and proposes a design methodology. The specific EPB configuration analyzed in this paper, denoted here Exposed Base Plate with Extended Anchor Bolts (EBP-EAB), is illustrated in Fig. 1. The base plate is welded to the bottom of the column and sits on a grout pad/concrete foundation. A steel chair plate and vertical stiffeners are provided to make possible a well-defined stretch length. The intention is to concentrate most of the nonlinear action (ideally all) in the anchor bolts (mainly in the extended region) while the other connection components remain elastic. The EBP-EAB has been, and is, extensively used in steel industrial buildings (Fig. 1c) in countries of high seismic activity (e.g., Chile, Peru). It has a suitable energy dissipation capacity [31], and repair times are short [32] after large earthquakes (e.g., 1960 Valdivia (Chile) $M_w = 9.2$; 2010 Maule (Chile) $M_w = 8.8$). Surprisingly, EBP-EABs have not received much attention in the research arena; in particular, the actual hysteretic characteristics of EBP-EABs have not been analyzed in detail.

In light of the presented background, the objectives of this paper are: 1) to develop sophisticated FE models to understand the essential characteristics of the behavior of EBP-EABs; 2) to validate the models against selected experimental tests reported in the literature; and 3) to present a methodology to design EBP-EABs. The details of the FE models are presented along with their respective validation. A subsequent section describes the results of the FE simulations and presents a design methodology for EBP-EABs. Finally, the paper concludes by outlining the limitations of the current work and by recommending specific future research endeavors.

2. Finite element models of EBP-EAB connections

As for any other type of column base connection, the response of EBP-EABs is controlled primarily by the behavior of their components and by the interactions between such components, e.g., contact/gapping between the base plate and the grout pad. Thus, these complex interactions are explicitly simulated in the FE models developed in this study. A total of sixteen three-dimensional (3D) models were created in the ABAQUS [33] simulation platform. For the objectives of this paper, these models were divided into two groups. In the first group (denoted as Group 1), the connection comprises a W200 × 71 (W8x48 imperial units) column section with base plate dimensions of 356 × 356 mm. Three levels of axial load were considered (i.e., 0.00, $0.10F_yA$, and $0.20F_yA$), along with two different free stretch lengths of the anchors (i.e., 290 mm and 150 mm) and two types of anchor bolts (i.e., cast-in smooth-shank, and bonded) are considered (a total of 12 models, see Table 1). The steel column section, the base plate dimensions, and the diameter of the anchor rods in Group 1 are equal to those of the CBCs tested by Gomez et al. [8] and by Trautner et al. [11], which make possible meaningful comparisons. Moreover, results from the Group 1 models provided the basis for a rational design procedure (presented later in this paper) intended to promote plastic strains only in the extended region of the anchor bolts. All models were subjected to the SAC cyclic load protocol [34] in the presence of an axial compressive force. Table 1 resumes the key model characteristics of Group 1.

The second group of models (denoted as Group 2) are designed based on the procedure presented later in this paper. These models are intended to provide more insight into the hysteretic characteristics of *designed* EBP-EABs and their potential incorporation into the energy dissipation mechanism of SMFs. Table 2 summarizes the relevant model characteristics of this group. In contrast with the Group 1 models, Group 2 models represent CBCs appropriate for mid-rise buildings, which is consistent with the engineering practice in industrial facilities. Thus, the validity of the design procedure presented later in Section 4 is examined

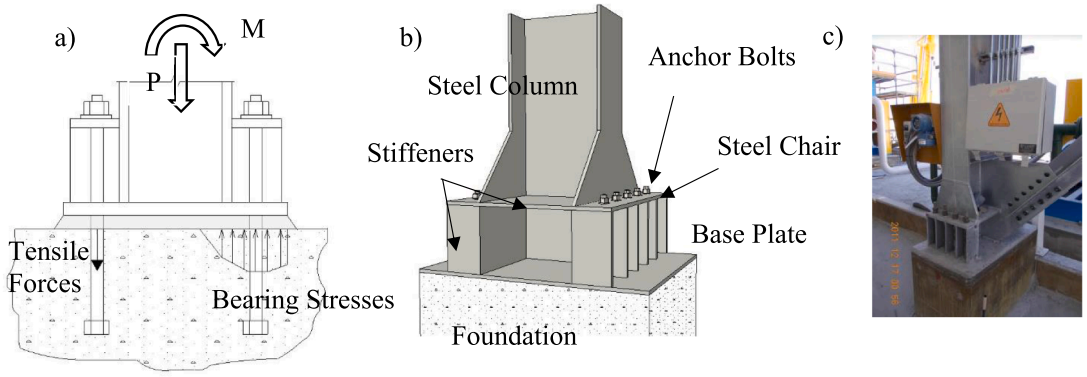

Fig. 1. Exposed Base Plate with Extended Anchor Bolts (EBP-EAB): a) side view, b) 3D view, c) Typical example in Chile.

Table 1
Details of Group 1 models.

Model	*B*(mm)	*N*(mm)	L_{sh}(mm)	*Bolt Type*	*Bolt Diameter* (in)[1]	P_u(kN)
P0EX290BA	356	356	290	Bonded	1.00	0
P10EX290BA	356	356	290	Bonded	1.00	320
P20EX290BA	356	356	290	Bonded	1.00	640
P0EX290HA	356	356	290	Smooth Shank	1.00	0
P10EX290HA	356	356	290	Smooth Shank	1.00	320
P20EX290HA	356	356	290	Smooth Shank	1.00	640
P0EX150BA	356	356	150	Bonded	1.00	0
P10EX150BA	356	356	150	Bonded	1.00	320
P20EX150BA	356	356	150	Bonded	1.00	640
P0EX150HA	356	356	150	Smooth Shank	1.00	0
P10EX150HA	356	356	150	Smooth Shank	1.00	320
P20EX150HA	356	356	150	Smooth Shank	1.00	640

[1] Four anchor rods in all cases.

Table 2
Details of Group 2 models.

Model	*B*(mm)	*N*(mm)	L_{sh}(mm)	*Bolt Type*	*Bolt Diameter* (in)	P_u(kN)
P5EX11HA	900	450	400	Bonded	1.50[2]	334
P10EX13HA	850	400	370	Bonded	1.25[2]	668
P15EX14HA	850	400	360	Bonded	1.00[3]	1002
P20EX14HA	850	400	360	Bonded	1.00[2]	1336

[2] Six anchor rods.
[3] Eight anchor rods.

through FE simulations. The only parameter varied in the Group 2 models is the axial load level (i.e., $0.05F_yA$; $0.10F_yA$; $0.15F_yA$; and $0.20F_yA$) since this variable plays a significant role in the behavior of the exposed base connections [8]. It is important to highlight that Group 2 models were sized considering a bending moment equal to $0.30M_p$ (Plastic Moment) of the attached column. In doing so, the intention is to avoid any failure mode associated with the column, forcing it to remain elastic essentially.

3. Details of the FE models

3.1. Description of the models

Fig. 2 shows a representative FE model of an EBP-EAB. All models were developed in the ABAQUS simulations platform [33]. These models were constructed using Hex-structured elements, and meshes were refined in places where stress concentrations were anticipated. The models include the nonlinear (geometric) effects of large deformations. The interfaces between the base plate and the grout pad, the washers and the top side of the steel chair, the anchor bolts and the base plate, the anchor bolts and the grout pad, and the anchor bolts and the concrete foundation were all simulated as a surface-to-surface contact with a finite sliding formulation. Normal and tangential contact interaction properties were assigned. The normal contact was defined as a *hard* contact, which allows separation after contact. The direct (Standard) method was selected as the constraint enforcement method. Friction formulations were adopted depending on the interacting components. Namely, for the base plate to grout pad contact, an isotropic friction formulation following the penalty method was defined with a coefficient of friction equal to 0.45 [8]. For the contact between metal elements, i.e., washer to the top side of the steel chair, anchor bolts to steel chair holes, and anchor bolts to base plate holes, the coefficient of friction was set equal to 0.80 [35]. In EBP-EABs with smooth anchor bolts, a frictionless formulation was assigned since experimental evidence indicates that this type of anchor bolt debonds along the embedded length [8,11]). In EBP-EABs with bonded anchor bolts, on the other hand, experimental evidence [11] supports a model where anchor bolts are tied to the concrete foundation. Other finite element modeling strategies (including simplified techniques) to simulate the displacements of anchor bolts embedded on concrete have been reported in the literature (e.

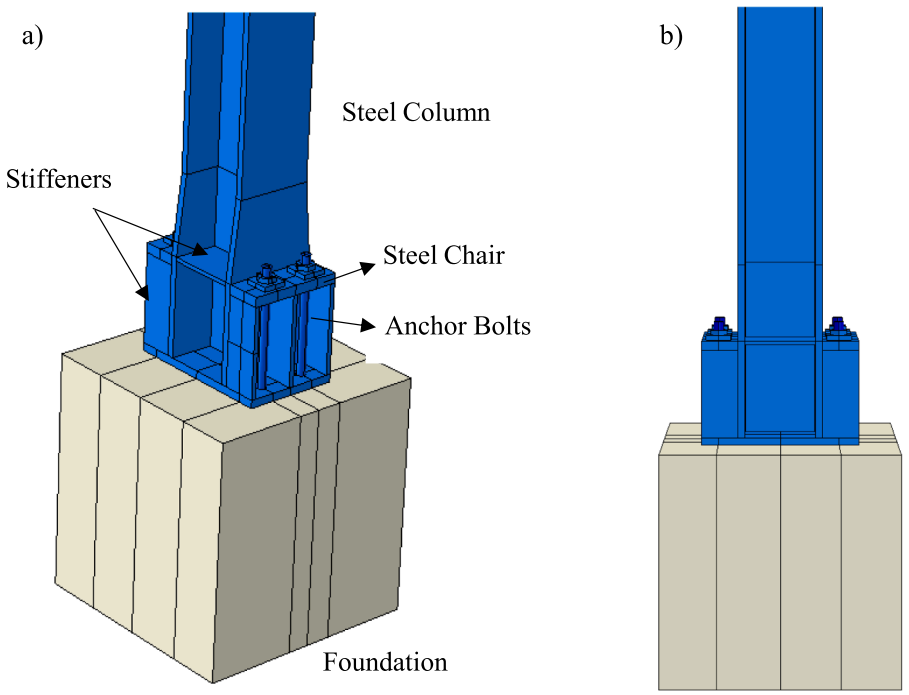

Fig. 2. Representative Finite Element model of EBP-EABs: a) 3-D view; b) Elevation view.

g., [22]). However, the assumptions made in this study (which are supported by experimental evidence) are deemed appropriate for the purposes of this investigation.

Contacts between the remaining components (i.e., steel chair to column flange, base plate to column bottom, stiffeners to column flange, stiffeners to the base plate, stiffeners to the steel chair, and base plate to shear key) were assumed monolithic since these components are welded and resist fracture. Finally, since no separation between the grout pad and the concrete foundation has been observed in experimental tests, tie constraints were also assigned to this interface.

The steel components of the EBP-EABs (i.e., column, base plate, anchor bolts, stiffeners, and steel chair) were modeled with the Von Mises material with isotropic strain hardening (including cyclic hardening). ASTM F-1554 Gr36 material was used for the anchor bolts, while the rest of the steel components were modeled using ASTM A992. The models were calibrated with the ancillary data reported in Gomez et al. [8]. True stresses and strains were assumed in the material formulation. The strain data reported in the ancillary tests conducted by Gomez et al. [8] was transformed into true strains using Eq. (1). True stress and plastic strains were obtained using Eqs. (2) and (3), respectively. In these equations, ε and σ are the experimental strains and stresses reported by Gomez et al. [8] from ancillary tests conducted on the mentioned materials, and E is the Young modulus. Concrete and grout were simulated with the concrete damage plasticity model [33]. Nuts and washers were idealized as linear-elastic elements since experimental evidence indicates that these pieces remain elastic during the tests.

$$\varepsilon_{true} = ln(\varepsilon + 1) \tag{1}$$

True stresses were computed by:

$$\sigma_{true} = \sigma(\varepsilon + 1) \tag{2}$$

Plastic strains were obtained from:

$$\varepsilon^{p}_{true} = \varepsilon_{true} - \frac{\sigma_{true}}{E} \tag{3}$$

The SAC lateral load protocol [34] was applied to all models. First, the axial load was applied and held constant, and then the lateral load protocol was applied at the top of the column. The axial load (including the self-weight of the connection) was applied strategically at the bottom of the column to avoid $P-\Delta$ effects (see Fig. 3). The quantities recorded from the simulations are the lateral force at the bottom of the foundation, the lateral displacement at the top of the column, forces in anchor bolts, and bearing stresses at the interface between the base plate and the grout pad. With this information, moment-rotation ($M-\theta$) curves of each connection were generated.

3.2. Model calibration

Validating computational models of CBCs using experimental data is an acceptable practice in the research arena (e.g., [9,36]). Trautner and Hutchinson [36] validated FE simulations of 30 experimental tests and found that the FE models effectively predict the response of CBCs. One of the tests from the experimental investigation conducted by Trautner et al. [11] (namely, specimen S2S4) was selected to validate the FE modeling approach adopted in this paper. This specific specimen (S2S4) was chosen because it includes a steel chair with extended anchor bolts, i.e., this specimen is similar (and comparable) to the EBP-EABs studied herein.

Specimen S2S4 tested by Trautner et al. [11] was then modeled using the approach presented in Section 3.1, and results were compared with the experimental results. The metric used to validate the FE model is the degree of agreement between the hysteretic curves (i.e., experimental vs. numerical). This validation criterion has been adopted in the past by other researchers (e.g., [9,17,18,36] since the hysteretic curves do include the key aspects that characterize the response of CBCs (i.e., yield and maximum strength, initial rotational stiffness, rotation capacity, and deterioration characteristics).

Fig. 4 illustrates the hysteretic response of the FE model of specimen S2S4. When compared with the experimental results reported in Trautner et al. [11], it is clear that the main characteristics of the response are indeed captured by the FE model (see Table 3). Specifically, the flag shape of the hysteresis loops, the absence of residual forces at zero rotations (which potentially suggests self-centering characteristics), and salient features such as the moment at first yield M_y, the initial rotational stiffness K_y, the peak strength M_{peak}, the rotation associated

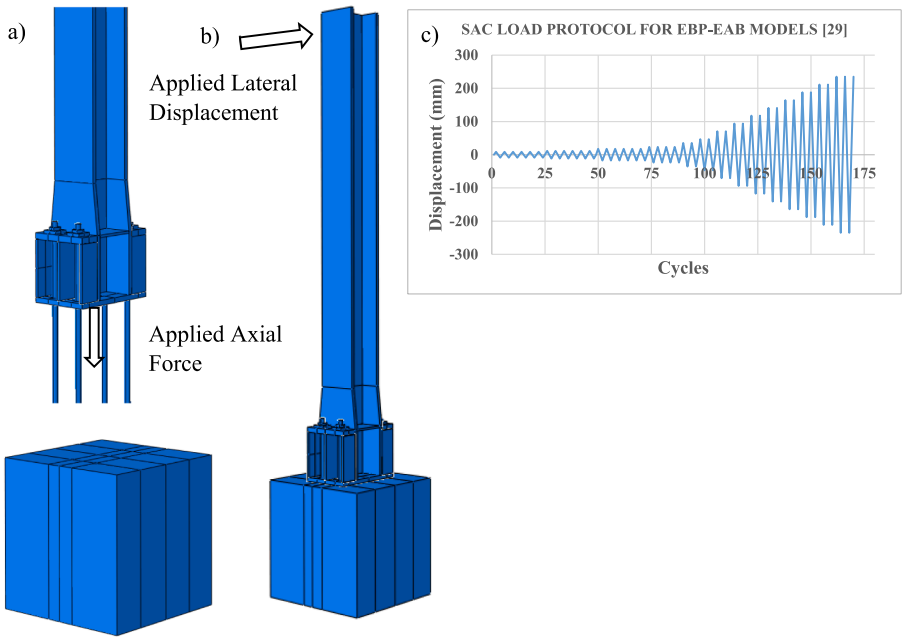

Fig. 3. Description of loading history for EBP-EAB models: a) Application of Axial Force; b) Application of Lateral Displacements; c) SAC Load Protocol [29].

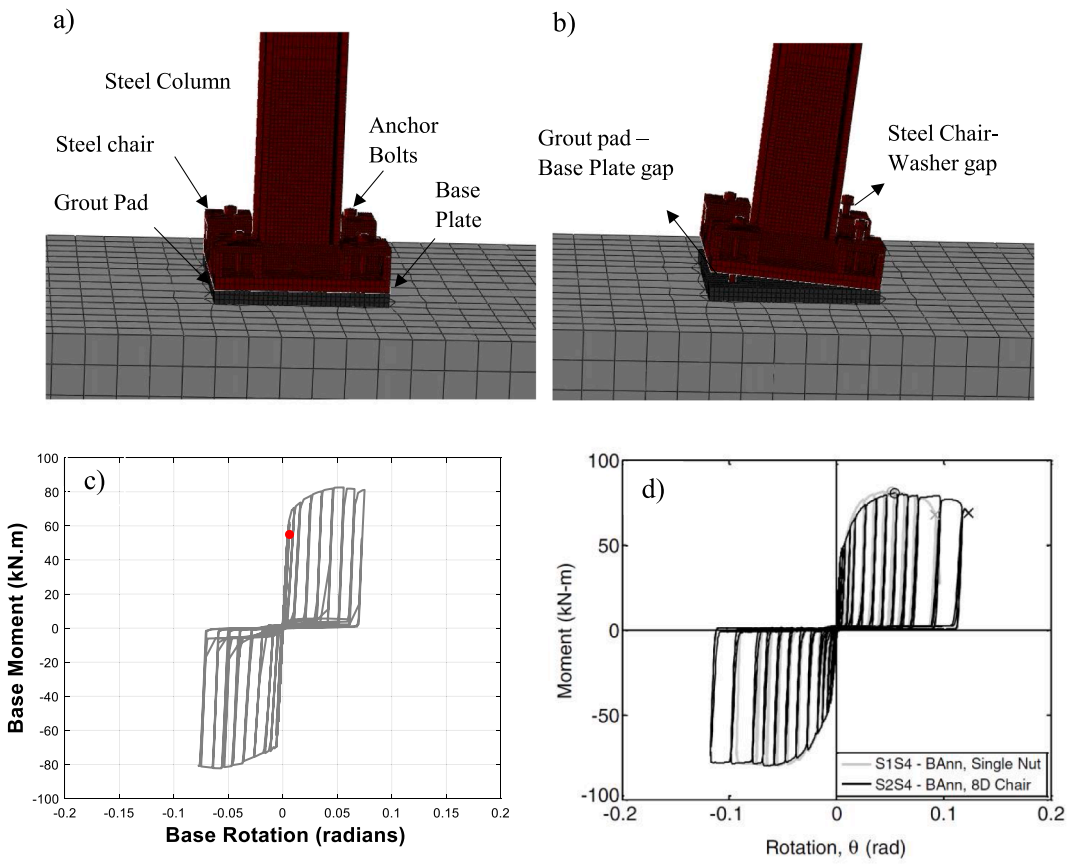

Fig. 4. Validation of the modeling procedure using specimen S2S4 tested by Trautner et al. [11]: a) undeformed shape; b) deformed shape; c) FE results; d) experimental results (reproduced from Trautner et al. [11]).

with M_{peak}, and the strength deterioration are all well captured. Fig. 4c indicates that specimen S2S4 exhibits a linear-elastic behavior up to a point associated with the first yield (red dot in Fig. 4c). Then, a nonlinear strain-hardening branch is observed. Strength deterioration is observed after the peak strength is reached. The values obtained from the FE model are very close to those obtained from the test. Moreover, it

Table 3
Model validation: specimen S2S4 tested by Trautner et al. [11].

Experimental Test (Trautner et al. [11])				
M_y	θ_y	k	M_{peak}	θ_{peak}
(kN m)	**(rad)**	**(kN m/rad)**	**(kN m)**	**(rad)**
48.00	0.005	9600.00	83.60	0.06
FE model				
M_y	θ_y	k	M_{peak}	θ_{peak}
(kN m)	**(rad)**	**(kN m/rad)**	**(kN m)**	**(rad)**
53.80	0.005	10760.00	81.88	0.06

is worth comparing the results from Fig. 4 with the study conducted by Park et al. [22] on the connection assembly with stretch length bolts for storage casks (similar to the EBP-EAB detail). As per this study, the connection response shows similar characteristics as those reported by Trautner et al. [11] and complements the model validation. Thus, in the authors' opinion, this validation provides enough confidence in the FE models developed in this study; consequently, these models are deemed reliable for this investigation.

3.3. Group 1 models: Analysis of results

3.3.1. General observations

Fig. 5 shows the moment vs. rotation relationship of the EBP-EAB models of Group 1. Results indicate that the EBP-EAB configuration has desirable hysteretic characteristics with a high deformation capacity (~0.10 rad). Furthermore, the flag shape characteristic of the hysteresis loops is observed in all cases, as well as the re-centering effect. As indicated before, the re-centering property is desirable since it is consistent with the global self-centering building behavior. Thus, it can be inferred from these numerical simulations that energy dissipation in EBP-EABs is stable. The hysteretic behavior of EBP-EABs might be conveniently divided into the following stages. The first stage is a well-defined linear elastic phase where rotations are small, and no damage is observed.

In contrast, the "standard" EBP presented in Design Guide 1, and tested by Gomez et al. [8], exhibits nonlinear behavior even at small deformations (Fig. 6). The first stage ends when the tensile anchor bolts yield, which is illustrated in Fig. 7. Immediately afterward, a sudden change in the slope of the curve is observed, characterized by strain-hardening and base rotations increase due to the uplifting of the base plate from the grout pad. In this stage, plastic strains in the tensile anchor bolts spread out through the exposed stretch length in smooth-shank and bonded rods. No plastic strains are observed in the other components of the EBP-EAB (i.e., base plate, steel chair, stiffeners, and steel column). The second stage ends at load reversal; hence the third stage is the unloading phase. It is observed that the unloading slope is similar to the initial slope. During this stage, the tensile anchor bolts relax while the base plate returns to its original position. This stage ends when the nut/washer arrangement loses contact with the top side of the steel chair. In the presence of axial loads, this loss of contact causes an intermediate plateau, as observed in Fig. 5. This intermediate plateau continues until the gap between the base plate and the grout pad is closed. It must be noted that these cyclic response characteristics may have important implications on the response to random time-varying loads such as seismic loads, but such implications are beyond the scope of this research and are left for further studies.

As per Fig. 5, no deterioration is observed up to rotations as high as ~ 0.07 rad. Two modes of cyclic deterioration are identified at larger rotations: 1) unloading stiffness deterioration and 2) re-loading stiffness deterioration. These deterioration phenomena could be attributed to the plastic strains in the anchor bolts accrued during the cyclic loading, while grout deterioration might also contribute.

3.3.2. Effect of the axial force

In the presence of axial compressive force, a clear intermediate plateau is observed in the moment-rotation curves. In contrast, in the models without axial load, this plateau essentially coincides with the horizontal axis (see Fig. 5). This phenomenon is most likely due to the axial compressive force delaying the loss of contact between the base plate and the grout pad. The same effect has been observed in the standard DG1 EBPs tested by Gomez et al. [8] and the EBP-ABYs tested by Trautner et al. [11]. Apart from its influence on the hysteretic shape, increasing axial forces lead to increases in three response quantities: the initial rotational stiffness, the Moment at First Yield, and the Peak Moment. Results shown in Fig. 5 also indicate that the axial load does not affect the rotation capacity of the EBP-EAB connection.

3.3.3. Effect of the type of anchor bolt

Results also indicate that the type of anchor bolt (i.e., bonded vs. smooth shanks) slightly affects the initial rotational stiffness and the peak strength of the connection. This effect is illustrated in Fig. 8 and is more prominent in EBP-EABs with smaller exposed lengths. The increment of initial rotational stiffness can be attributed to the reduction of the effective stretch length caused by the adhesive bond. This smaller length entails that the plastic strains are concentrated mainly in the free length of the anchor bolts. As illustrated in Fig. 9, when the anchor bolts are bonded, no plastic strains penetrate the concrete foundation. On the other hand, in the smooth shank bolts, plastic strains penetrate along the foundation depth. In the latter case, however, maximum strains are still located at the free length. Thus, the deformation capacity of EBP-EABs seems to be practically insensitive to whether the anchor bolts are bonded or smooth shank, as long as the anchor bolts have the same elongation capacity.

3.3.4. Effect of the stretch length

A comparison between the first (i.e., stretch length = 290 mm) and second (i.e., stretch length = 150 mm) sets of plots in Fig. 5 indicate that the overall behavior of EBP-EABs is relatively insensitive to the stretch lengths considered in this paper (i.e., 290 mm and 150 mm). The only exceptions are the models in which the axial load is equal to $0.20FyA$. This observation is consistent with the experimental finding presented in Parks et al. [22] in single anchor experiments under combined tension and shear. The hysteresis curves of models P20EX290 are qualitatively identical to those of models P10EX290. The hysteresis curves of models P20EX150, on the other hand, are different from those of models P10EX150 in that the flag shape exhibits a more narrow intermediate plateau. This is most likely because, in these models, plastic deformations develop not only at the anchor bolts but also at the column web, which in turn seems to be a consequence of oversized anchor bolts.

A closer inspection of the strains in the anchor bolt reveals additional interesting findings. Strains in the anchor bolts monitored at column rotations equal to 0.04 rad and 0.10 rad are summarized in Table 4. It can be noted that at 0.04 rad (AISC341-16 target rotation for beam-column connections of SMFs), the anchor bolts in tension reach strains that are smaller than 0.10. This observation suggests that the anchor rods still have a suitable elongation capacity at 0.04 rad. However, important differences can be appreciated among the different stretch lengths and types of anchor bolt (i.e., headed vs. bonded anchor). For instance, at column rotations equal to 0.04 rad, the strains in the anchor bolts range between 0.019 and 0.081 in the models with a stretch length of 150 mm, whereas they range between 0.012 and 0.039 in the models with a stretch length of 290 mm. At column rotations equal to 0.10 rad, on the other hand, strains in the anchor bolts range between 0.050 and 0.380 and 0.070–0.142, respectively. Thus, the type of anchor bolt (smooth shank vs. bonded bolt) significantly influences the strains in the anchor bolts. Results shown in Table 4 indicate that strains in bonded anchor bolts are 3 to 5 times greater than those in headed anchor bolts. These findings directly impact the practical aspects of proportioning anchor rods for the design of EBP-EABs. When the stretch length L_d =

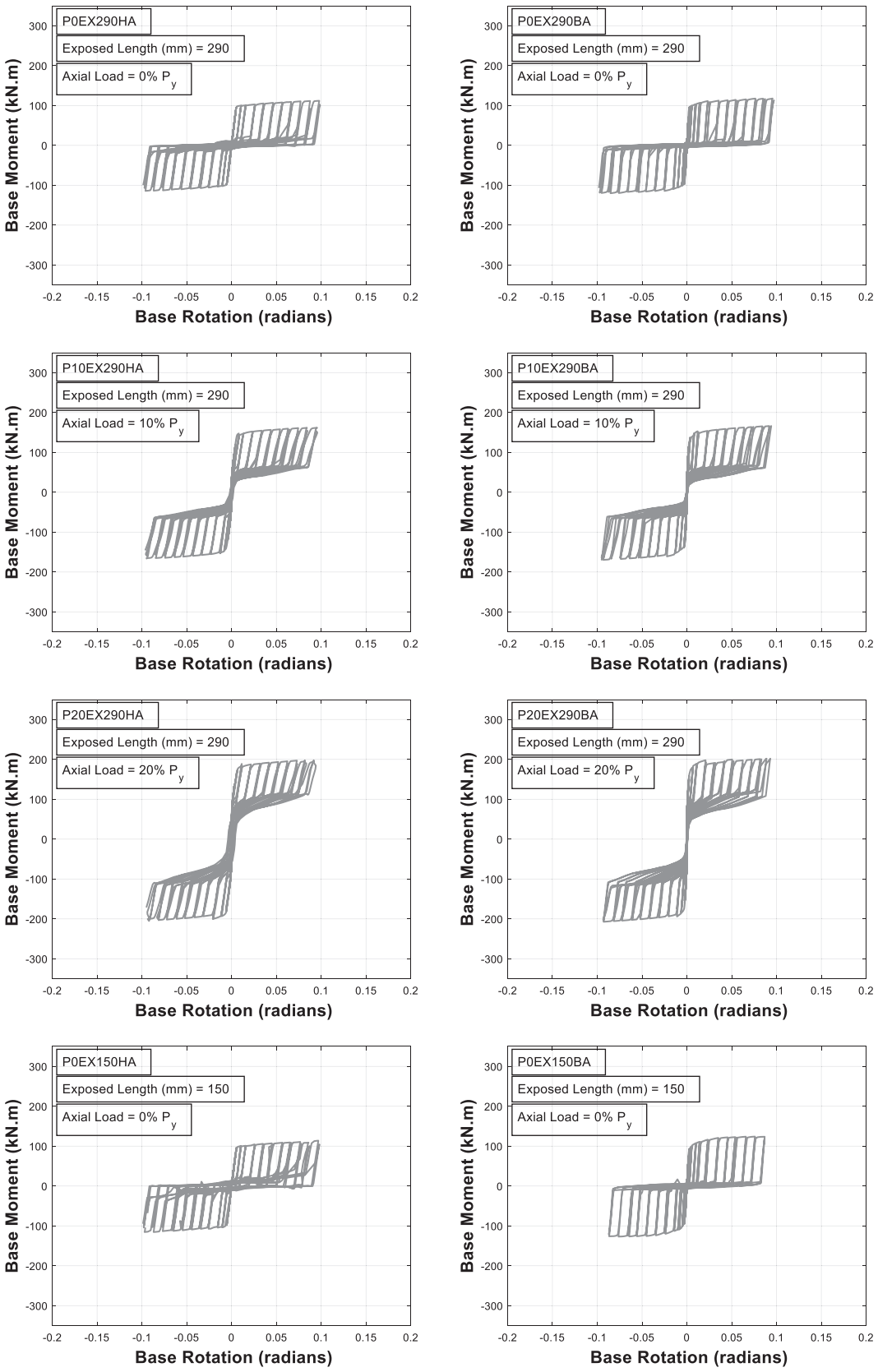

Fig. 5. Cyclic response of Group 1 FE models.

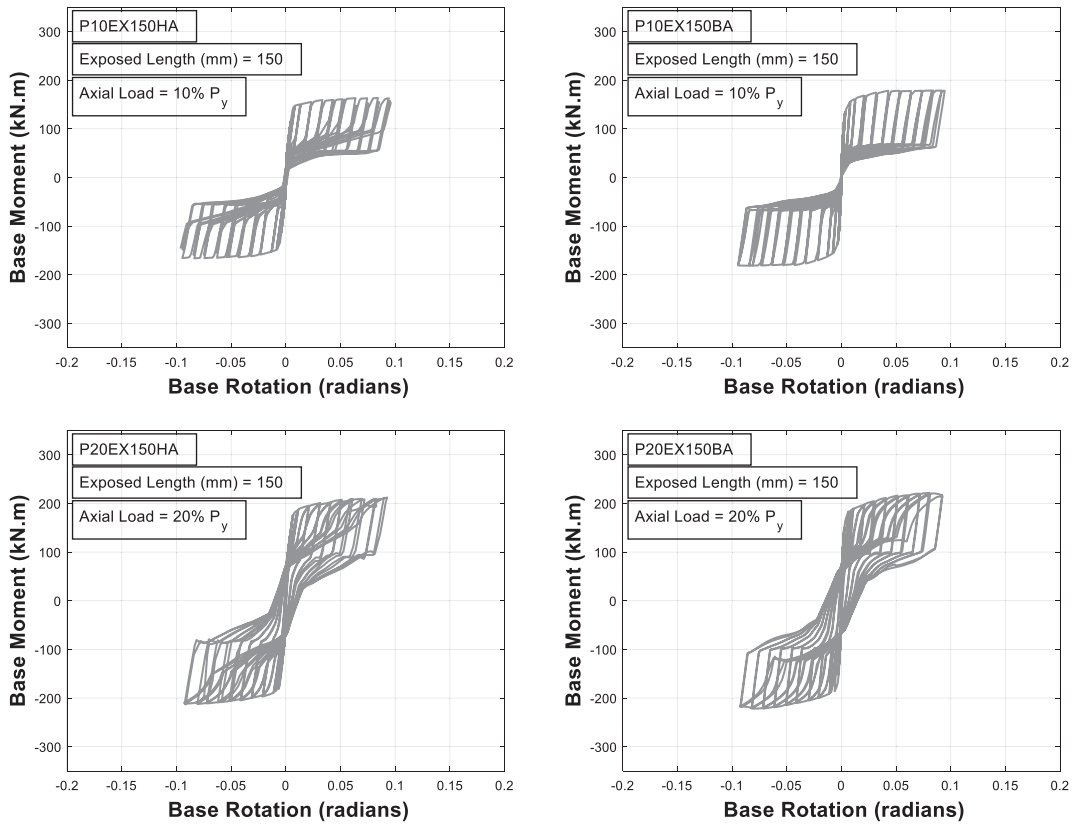

Fig. 5. (*continued*).

Fig. 6. Experimental hysteretic curve of a typical Design Guide 1 CBC (Gomez et al. [8]).

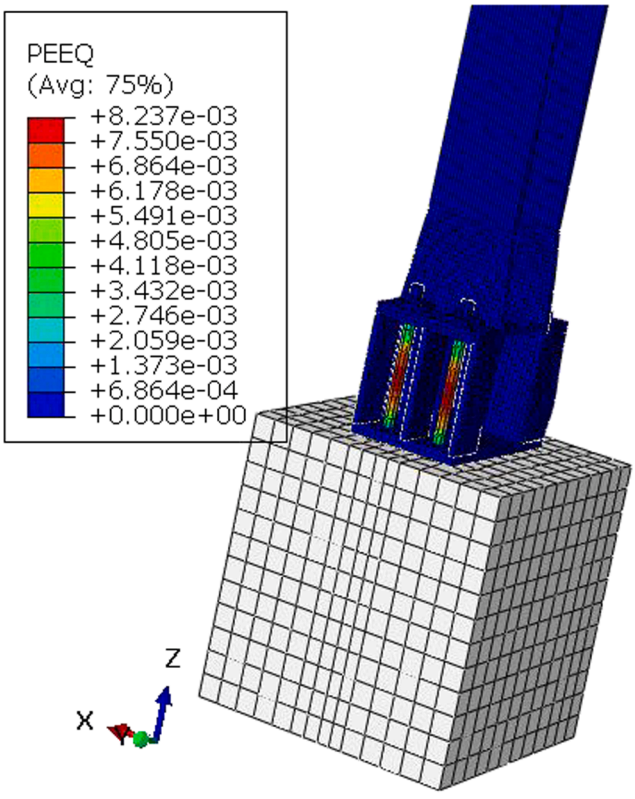

Fig. 7. Visual representation of the first anchor yielding in EABP-EAB models.

150*mm*, the aspect ratio (defined as L_d/d_{bolt}) is equal to 5.7; in contrast, an $L_d = 290mm$ results in an aspect ratio equal to 11.50. The latter is conforming to the design guidelines outlined in the commentaries to Chapter 17 of ACI 318–19 [37], where it is suggested that an $L_d/d_{bolt} = 8$ results in good performance based on field observations after earthquakes.

4. Suggested design procedure

Building on the insights gained from the FE simulations, a practical procedure for designing EBP-EABs aimed at concentrating plastic strains

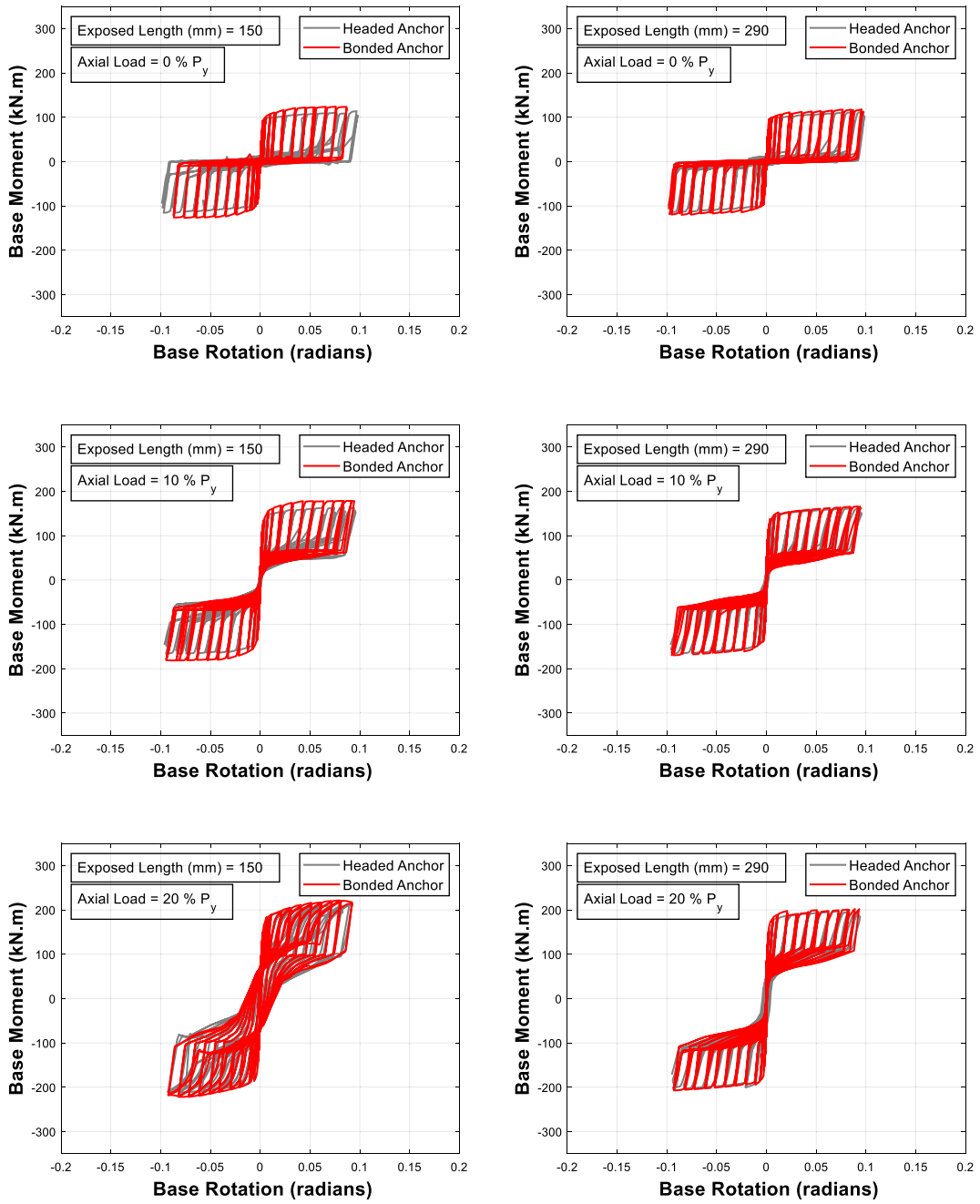

Fig. 8. Comparison between Bonded and Headed cyclic response in EABP-EAB models (Group 1, W8x48 Column).

in the free length of the anchor bolts is proposed. The design procedure leverages key aspects from DG1 (i.e., bearing stress block) and incorporates insights obtained in the previous section. The procedure is illustrated in Fig. 10 and summarized in the following steps:

1) The internal forces are characterized by the method presented in DG1. This method assumes that a combination of bearing stresses and anchor bolt forces resist the demand actions (M, P). Thus, the anchor bolt forces and the length of the bearing stress block are determined by solving the equilibrium equations (i.e., Eqs. (3) and (4) in DG1).
2) The forces in the anchors calculated in the previous step define the total required steel area of bolts.
3) A target rotation (e.g., 0.02 rad, 0.04 rad) and a maximum design anchor bolt strain are set to define the free stretch length and the anchor bolt diameter. For design purposes, a maximum anchor bolt strain of 0.10 is considered in this study, avoiding or limiting an eventual anchor rupture. Additionally, it is convenient to assume a rigid base plate rotation to compute the axial strains in the anchor bolts. Designs tested in this study (i.e., Group 2 models) were obtained considering a target rotation equal 0.04 rad. The exposed length was assumed to span from the bottom of the base plate up to the anchor nuts, as indicated in ACI318-19 [37]. Then, the stretch lengths were set equal to the greater of a) the length needed to achieve the target rotation and b) eight times the anchor rod diameter (as recommended in ACI 318–19 [37]). The stretch length proposed herein seeks to avoid brittle behavior (i.e., anchor bolts fracture) after rotations greater than 0.04 rad.
4) Once the anchor bolts are selected, the remaining components are calculated based on capacity design principles. The anchor rod capacity is computed according to Eq. (4).

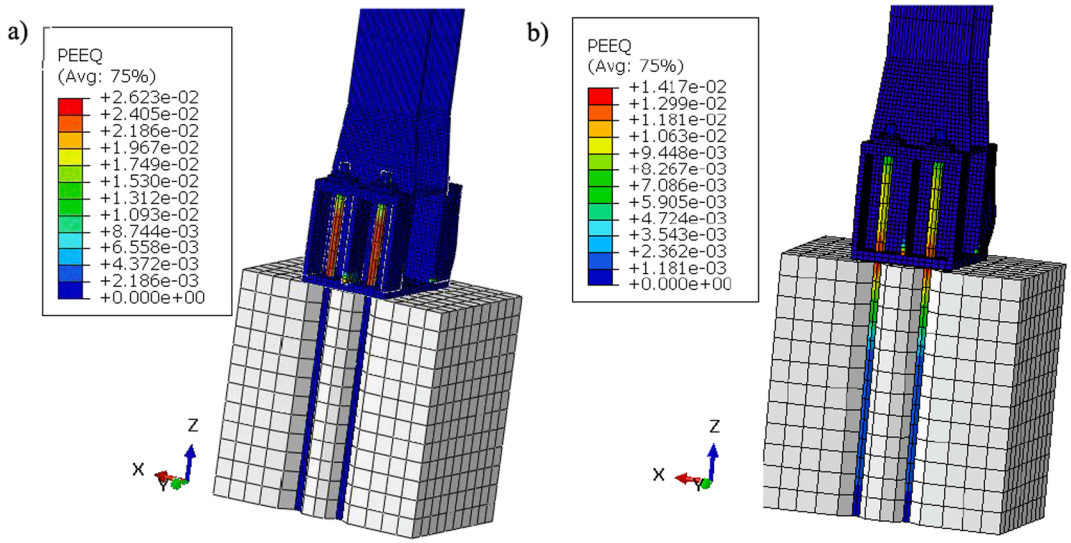

Fig. 9. Visual representation of plastic strains in anchor bolts in EABP-EAB models: a) bonded bolts; b) cast-in smooth-shank.

Table 4
Strains in anchor bolts (Group 1 models).

Model	ε(at 4 % rad)	ε(at 10 % rad)
P0EX290BA	0.0395	0.1420
P10EX290BA	0.0379	0.1110
P20EX290BA	0.0211	0.1020
P0EX290HA	0.0120	0.0699
P10EX290HA	0.0185	0.0758
P20EX290HA	0.0174	0.0710
P0EX150BA	0.0958	0.3760
P10EX150BA	0.0810	0.2320
P20EX150BA	0.0362	0.1610
P0EX150HA	0.0211	0.0732
P10EX150HA	0.0190	0.0880
P20EX150HA	0.0196	0.0500

$$T_u^{bolt} = R_y F_y A_g \geq 0.75 F_u A_g \tag{4}$$

5) The steel chair (or secondary plate) and the base plate are designed based on yield line theory with appropriate boundary conditions. This procedure is illustrated in Fig. 11. Thus, the thickness of these components is computed using Eqs. (5)–(10). In these equations, f_{max} is calculated using Eq. (5) considering amplified forces or concrete strength (the latter is considered in this study), a and b are the free edge width and the dimension perpendicular to the free edge width, e_{bp} and e_{sc} are the base plate and steel chair thicknesses, respectively, d_{hole} is the diameter of the hole of either the base plate or the steel chair, and k_{bp} and k_{sc} are the yield line factors for the base plate and steel chair, respectively.

Base plate:

$$P_u = f_{max} ab \tag{5}$$

$$\varnothing P_n = \varnothing \frac{e_{bp}^2}{4} F_y k_{bp} \tag{6}$$

$$k_{bp} = \frac{12}{5}\left[\frac{6}{b}\left(a - \frac{2d_{hole}}{3}\right) + \frac{4}{a}\left(b - \frac{d_{hole}}{2}\right)\right] \tag{7}$$

Steel chair:

$$P_u = T_u^{bolt} \tag{8}$$

$$\varnothing P_n = \varnothing \frac{e_{sc}^2}{4} F_y k_{sc} \tag{9}$$

$$k_{sc} = \frac{6}{b}\left(a - \frac{2d_{hole}}{3}\right) + \frac{2}{a}\left(b - \frac{d_{hole}}{2}\right) \tag{10}$$

6) Finally, the steel chair stiffeners are designed to hold a compressive force greater than a) anchor bolt capacity (Eq. (4)) and b) the maximum reaction at the interface between the base plate and the grout pad.

Dimensions a and b, and therefore the corresponding width and length (N and B) of the base plate, are defined based on erection tolerances. In this study, a minimum of four times the anchor bolt diameter is considered as the anchor to edge distance. Table 5 shows a comparison between values of key parameters obtained from the FE simulations and the proposed design procedure. These values were obtained from the Group 2 models, which were designed per the proposed procedure. As mentioned before, these models are representative of CBCs in mid-rise industrial buildings. It is important to point out that the EBP-EAB design procedure presented herein does not establish a fixed value of the stretch length, as indicated in different codes (e.g., [37,38]). Rather, the defined target rotation guides the estimation of stretch length. Although the stretch length could be considered a design parameter, the rotation is directly related to the expected performance. Further, setting the rotation value is consistent with the philosophy of pre-qualified beam-column connections as stated by AISC 358–16 [39]. Thus, the rotation capacity of CBCs should be estimated considering either the stretch length of the anchor or the anchors' embedded deformable portion. The latter is not commonly indicated in design codes (e.g., [37,38]).

Additionally, the authors expect this procedure to remain valid if post-installed anchor bolts are used in the EBP-EAB detail as long as their ductility characteristics are comparable with those analyzed in this paper. Previous experimental research on the topic [12] indicates that all thread post-installed bonded anchors pose significant ductility. Thus, from the author's point of view, post-installed anchor bolts can be used as a construction alternative to increase the efficiency of the construction process by reducing alignment problems *in situ*. Moreover, this solution can be useful for retrofit purposes after a large earthquake event. However, from this perspective, various solutions for retrofit purposes can be thought of, and each of them can affect the connection

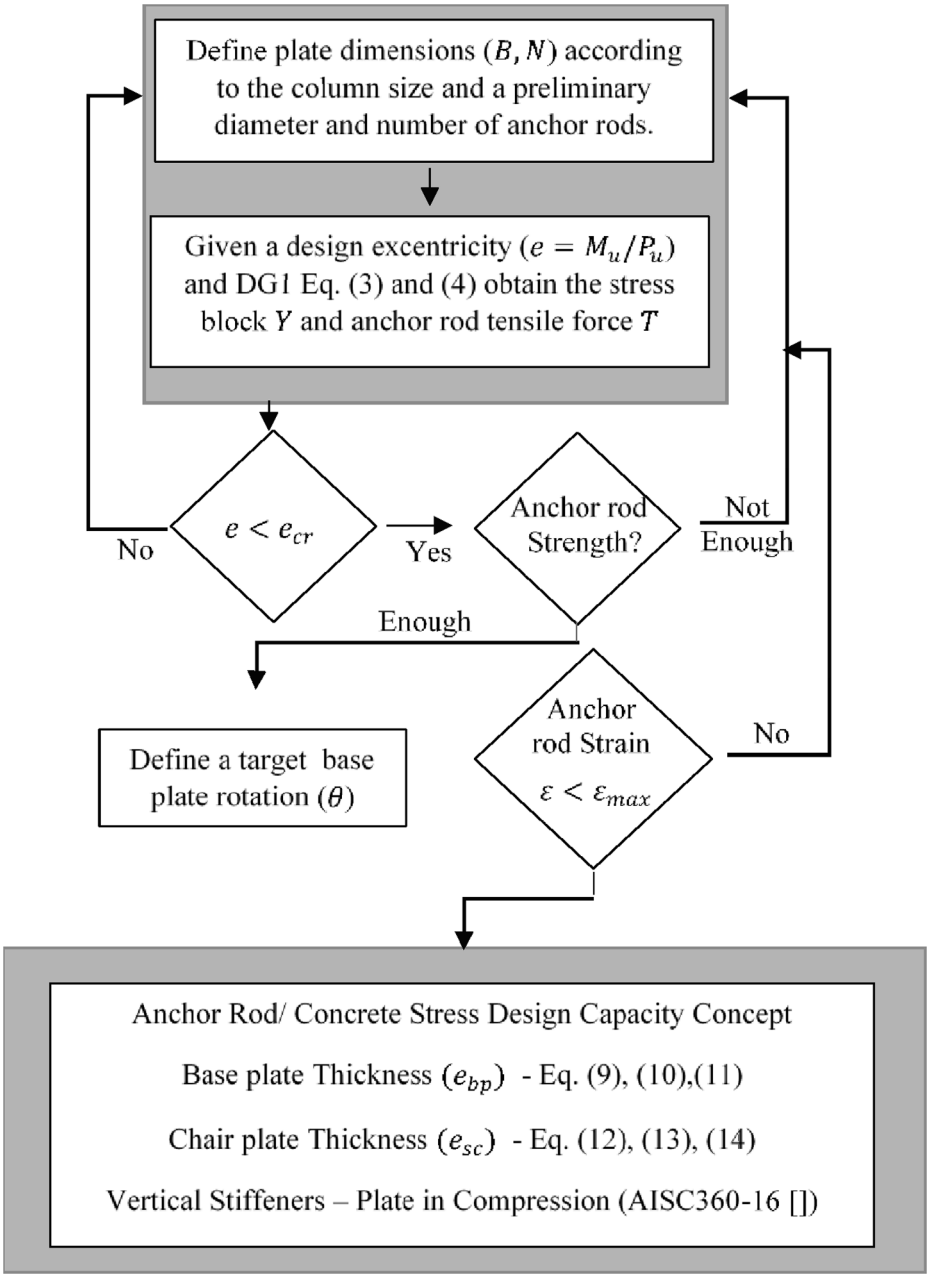

Fig. 10. Flow chart for the proposed EABP-EAB design procedure.

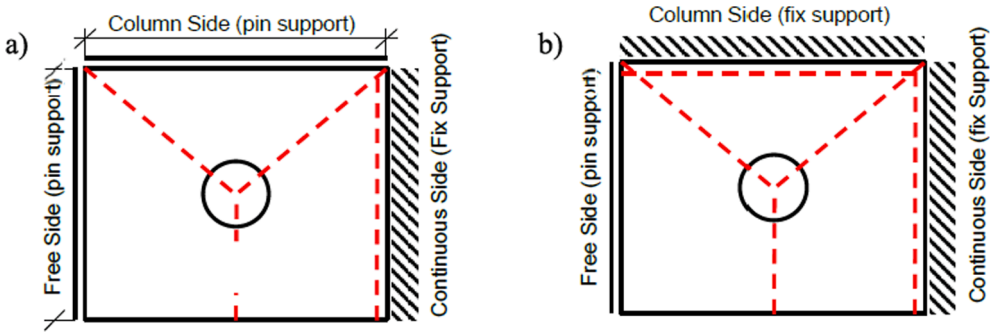

Fig. 11. Influence line for the design of EABP-EAB connections for a) steel chair; b) base plate.

Table 5
Estimation of design parameter in Group 2 EBP-EAB connections.

Model	ABAQUS			ANALYTICAL			ERROR		
	M_y(kN m)	M_u(kN m)	k(kN m/rad)	M_y(kN m)	M_u(kN m)	k(kN m/rad)	ε_y^*	ε_u	ε_k
P5EX11HA	93.70	111.78	18372.55	78.00	113.80	17172.00	1.20	0.98	1.07
P10EX13HA	95.00	117.16	32758.00	78.00	113.80	25307.00	1.22	1.03	1.29
P15EX14HA	140.50	161.61	23416.00	135.57	167.80	21579.00	1.04	0.96	1.09
P20EX14HA	137.47	166.18	38391.00	135.57	167.80	28131.00	1.01	0.99	1.36

performance differently. For instance, the use of infill materials in the anchor bolts embedded in the post-installed anchor assemblies may affect their deformation response and, consequently, the connection performance. Because of it, further research is required on the connection performance utilizing different anchor bolts assemblies.

5. Group 2 models: Analysis of results

Fig. 12 shows the moment vs. rotation relationship of the EBP-EAB models of Group 2 (i.e., designed using the proposed design procedure). It can be observed that the performance of EBP-EABs designed per the procedure presented in Section 4 is similar to that of the Group 1 models. Further, results also indicate that the plasticity is concentrated at the free stretch length of the anchor bolts, and no plastic strains develop in the column, validating the proposed design procedure. These models achieve rotations of up to 0.10 rad without appreciable loss of strength. In addition, the flag shape of the hysteretic loops and the re-centering effect are observed in all the simulations. Similar to what was done in the Group 1 models, different axial load levels were considered for component performance assessment. As illustrated in Fig. 12, the axial load level affects the core parameters of the backbone curve. Thus, larger axial loads entail larger rotational stiffness and larger strength, similar to what was observed in the hysteresis curves of the Group 1 models.

Results presented in this paper suggest that the EBP-EAB detail for a base connection could be advantageous over the common DG1 design. For instance, the concentration of plastic strains in the anchor bolts rather than in the lower region of the column is a suitable alternative solution to protect the column against undesired shortening phenomena during inelastic incursions. Furthermore, results suggest that an optimum proportioning of EBP-EAB can balance the potential flexibility of the connection and its energy dissipation capacity. This criterion might entail EBP-EABs to become proper fuses that can add energy dissipation to the building without spreading the damage to other components such as the first story columns.

Moreover, the extended length of anchor bolts makes post-earthquake inspections easier since damage (or, rather, the inelastic elongations) can be easily observed. Further, repairs are easier, particularly when the level of damage is small. For instance, the nuts can be re-tighten if the inelastic deformations are smaller than a pre-defined limit (defined by the designer). Alternatively, the anchor bolts can be removed without modifying the first story column (replaceable anchor rods could be considered at the design stage). The analytical cyclic response of the EBP-EABs designed as proposed in this study indicate that the idea of avoiding damage in the first story columns can be achieved in practice.

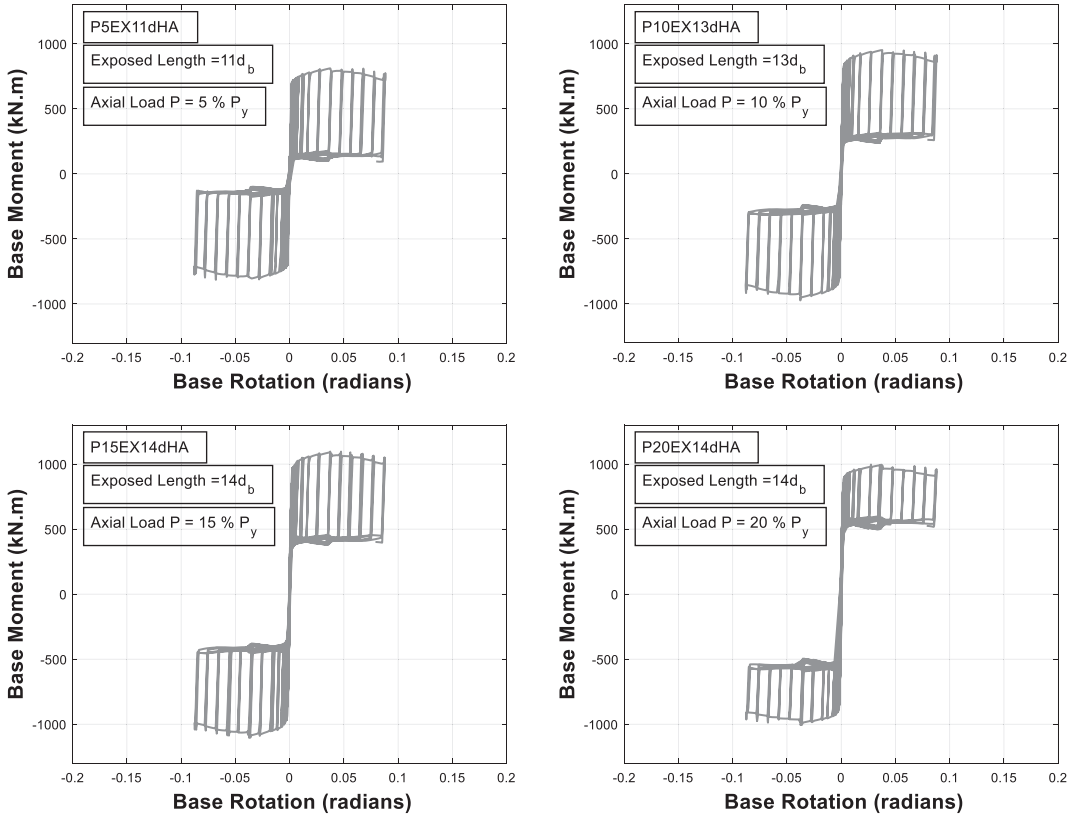

Fig. 12. Cyclic response of Group 2 FE models.

6. Summary, limitations, and conclusions

This paper presents a study on the cyclic response of a particular type of column base connection (CBC), namely the exposed base plate with extended anchor bolts (EBP-EAB). EBP-EABs have been used in industrial buildings for a long time in countries of high seismic activity (e.g., Chile and Perú) and performed well under strong earthquakes (e.g., the 2010 Chile earthquake). However, although the EBP-EAB is described as a suitable base plate configuration in modern codes (e.g., [37]), relevant information on its seismic behavior is, to the best of the authors' knowledge, absent in the literature. As a result, practitioner engineers use *ad hoc* design methods based on research on similar CBCs. Thus, the need to determine the actual behavior of the EBP-EAB and develop a proper design methodology based on a scientific background is real and timely.

A series of nonlinear FE simulations constitute the scientific basis of this investigation. Sixteen FE models were developed to study the behavior of EBP-EABs and were divided into two groups. The first group consists of models whose dimensions are consistent with CBCs tested in past research [8,11]. Results from the first group of models provide insight into the effect of different variables (i.e., stretch length, axial load level applied, type of anchor bolt) on the cyclic response. It was found that EBP-EABs have excellent dissipation and deformation capacities and do not exhibit important stiffness or strength degradation. Although the global response is relatively insensitive to the stretch length, the level of strains in the anchor bolts does depend heavily on the stretch length. A similar observation applies to the type of anchor bolt. In general, bonded bolts seem to provide higher rotational stiffness, but at the expense of higher strains in the bolts.

Based on the insights obtained from the first group of models, a design procedure for EBP-EABs is proposed. The proposed design procedure intends to concentrate all the plastic strains in the extended region of the anchor bolts, forcing the other components to remain elastic. In doing so, damage in the first story column is avoided, and post-earthquake repairs, if needed, are neither expensive nor time-consuming. To validate this design procedure, the second group of models was developed. They were designed per the proposed method and are representative of EBP-EABs in real mid-rise industrial buildings. Results obtained from these models indicate that the proposed design methodology leads to EBP-EABs having desirable cyclic behavior and suitable hysteretic properties. Thus, it is concluded that well-designed EBP-EABs have two important characteristics. The first one is related to the failure mechanism: plastic strains develop exclusively in the anchor rods, and no damage is expected at the remaining components. The second characteristic is the exposed stretch length, with which it is possible to achieve a target design rotation without significant strain concentrations in the anchor rods. The second characteristic facilitates post-earthquake inspections and repairs, and damage is virtually eliminated in the first story.

Based on the results from the FE simulations conducted in this paper, it is expected (in the authors' opinion) that EBP-EABs can potentially improve the seismic performance of SMFs. EBP-EABs can be modeled with a rotational spring using an appropriate phenomenological model similar to models developed by Torres-Rodas et al. [17] for exposed base plates. Furthermore, studies conducted in the past ([2,3,19]) indicate that the seismic demands on CBCs can be safely reduced if their hysteretic characteristics are accounted for when assessing the overall SMF behavior. Naturally, though, CBCs designed for lesser forces are more flexible. Hence, if the energy dissipation of the EBP-EABs is explicitly taken into account at the design stage, it will be necessary to find a proper balance between the seismic design forces and the flexibility of the EBP-EABs. This topic deserves further research and is beyond the scope of this paper.

The findings presented in this study rely on numerical simulation results that depend on the calibration of a single test. Other experimental programs with objectives similar to those of this investigation [21,22,40] confirm the findings presented herein about the benefits of plastic strain concentration in the stretch length of the anchor bolts, and further support the authors' analyses. Therefore, it is advised to realize the conclusions presented with a clear understanding of the assumptions. Furthermore, the authors encourage researchers to conduct large-scale experimental programs on EBP-EABs. Nevertheless, in the authors' opinion, the design method proposed herein provides practitioner engineers with a scientifically validated approach (to the extent possible) to design ductile base connections with extended anchor bolts.

CRediT authorship contribution statement

Pablo Torres-Rodas: Conceptualization, Data curation, Formal analysis, Investigation, Methodology, Project administration, Resources, Software, Validation, Visualization, Writing – original draft, Writing – review & editing. **Miguel Medalla:** Conceptualization, Data curation, Formal analysis, Investigation, Methodology, Project administration, Resources, Validation, Visualization, Writing – review & editing. **Farzin Zareian:** Conceptualization, Investigation, Methodology, Supervision, Validation, Visualization, Writing – review & editing. **Diego Lopez-Garcia:** Conceptualization, Investigation, Methodology, Supervision, Validation, Visualization, Writing – review & editing.

Declaration of Competing Interest

The authors declare that they have no known competing financial interests or personal relationships that could have appeared to influence the work reported in this paper.

Acknowledgements

Financial support was provided by the Research Center for Integrated Disaster Risk Management (CIGIDEN) ANID FONDAP 15110017 (Santiago, Chile). This support is gratefully acknowledged. The second author thanks the Ph.D. scholarship awarded by the National Commission for Scientific and Technological Research CONICYT through the program CONICYT-PCHA/Doctorado Nacional/2015-21150709. The authors also thank Miss Niloufar Behboud, Ph.D. (c), for her advice on the development of the FE models.

References

[1] Zareian F, Kanvinde A. Effect of column-base flexibility on the seismic response and safety of steel moment-resisting frames. Earthquake Spectra 2013;29(4):1537–59. https://doi.org/10.1193/030512EQS062M.
[2] Falborski T, Torres-Rodas P, Zareian F, Kanvinde A. Effect of Base-Connection Strength and Ductility on the Seismic Performance of Steel Moment-Resisting Frames. J Struct Eng 2020;146(5):04020054. https://doi.org/10.1061/(asce)st.1943-541x.0002544.
[3] Torres-Rodas P, Flores F, Pozo S, Astudillo BX. Seismic performance of steel moment frames considering the effects of column-base hysteretic behavior and gravity framing system. Soil Dyn Earthquake Eng November 2020;2021(144):106654. https://doi.org/10.1016/j.soildyn.2021.106654.
[4] Inamasu H, Lignos DG, Kanvinde AM. Effect of Column Base Flexibility on Earthquake-Induced Residual Deformations of Steel Columns. Key Eng Mater 2018;763:149–56. https://doi.org/10.4028/www.scientific.net/kem.763.149.
[5] Astaneh A, Bergsma G, Shen JH. Behavior and design of base plates for gravity, wind and seismic loads. In: Proceedings of the national steel construction conference, AISC Chicago, IL; 1992.
[6] Burda JJ. Studies of seismic behavior of steel base plates. Technical Report CCEER-99-7. University of Nevada, Reno; 1999.
[7] DeWolf J, Sarislay EF. Column ase plates with axial loads and moments. J Struct Division 1980;106(11):2167–84.
[8] Gomez I, Kanvinde A, Deierlein GG. Exposed Column Base Connections Subjected to Axial Compression and Flexure. Chicago: AISC; 2010. p. 257.
[9] Kanvinde AM, Jordan SJ, Cooke RJ. Exposed column base plate connections in moment frames - Simulations and behavioral insights. J Constr Steel Res 2013;84:82–93. https://doi.org/10.1016/j.jcsr.2013.02.015.
[10] Kanvinde AM, Higgins P, Cooke RJ, Perez J, Higgins J. Column Base Connections for Hollow Steel Sections: Seismic Performance and Strength Models. J Struct Eng 2015;141(7):04014171. https://doi.org/10.1061/(asce)st.1943-541x.0001136.
[11] Trautner CA, Hutchinson T, Grosser PR, Silva JF. Effects of Detailing on the Cyclic Behavior of Steel Baseplate Connections Designed to Promote Anchor Yielding.

J Struct Eng 2016;142(2):04015117. https://doi.org/10.1061/(asce)st.1943-541x.0001361.
[12] Trautner CA, Hutchinson T, Grosser PR, Silva JF. Investigation of Steel Column-Baseplate Connection Details Incorporating Ductile Anchors. J Struct Eng 2017;143(8):04017074. https://doi.org/10.1061/(asce)st.1943-541x.0001759.
[13] Drake RM, Elkin SJ. Beam-column base plate design-LRFD method. Eng J-Am Institute Steel Construct 1999;36:29–38.
[14] Fisher; James M. Base Plate and Anchor Rod Design. Steel Design Guide 1. AISC; 2006.
[15] Malley JO. AISC seismic design manual: Moment frames. Struct Congress 2007. https://doi.org/10.1061/40946(248)31.
[16] Kanvinde AM, Grilli DA, Zareian F. Rotational Stiffness of Exposed Column Base Connections: Experiments and Analytical Models. J Struct Eng 2012;138(5):549–60. https://doi.org/10.1061/(asce)st.1943-541x.0000495.
[17] Rodas PT, Zareian F, Kanvinde A. Hysteretic Model for Exposed Column-Base Connections. J Struct Eng 2016;142(12):04016137. https://doi.org/10.1061/(asce)st.1943-541x.0001602.
[18] Torres-Rodas P, Zareian F, Kanvinde A. A hysteretic model for the rotational response of embedded column base connections. Soil Dyn Earthquake Eng 2018;115:55–65.
[19] Inamasu H, Castro e Sousa A, Güell G, Lignos DG. Anchor-yield exposed column bases for minimizing residual deformations in seismic-resistant steel moment frames. Earthquake Eng Struct Dyn 2021;50(4):1083–100.
[20] Trautner C, Hutchinson T, Copellini M, Grosser P, Bachman R, Silva J. Developing Ductility using Concrete Anchorage. ACI Struct J 2017;114(1). https://doi.org/10.14359/51689152.
[21] Parks JE, Pantelides CP, Ibarra L, Sanders DH. Stretch length anchor bolts under combined tension and shear. ACI Struct J 2018;115(5):1317–28.
[22] Parks J, Pantelides CP, Ibarra L, Sanders DH. Cyclic tests and modeling of stretch length anchor bolt assemblies for dry storage casks. ACI Struct J 2020;117(6):225–36.
[23] Saleem M, Gutierrez H. Using artificial neural network and non-destructive test for crack detection in concrete surrounding the embedded steel reinforcement. Struct Concrete 2021;22(5):2849–67.
[24] Saleem M, Hosoda A. Latin hypercube sensitivity analysis and non-destructive test to evaluate the pull-out strength of steel anchor bolts embedded in concrete. Construct Build Mater 2021;290.
[25] Soules J, Bachman R, Silva J. Report of ASCE/SEI industrial assessment team on earthquake damage to industrial facilities in the conception area resulting from the chile earthquake of February 27, 2011. Reston, VA: ASCE; 2012.
[26] American Concrete Institute. Building Code Requirements for Structural Concrete ACI 318-11. ACI; 2011.
[27] American Institute of Steel Construction. Seismic provisions for structural steel buildings ANSI/AISC 341-16. AISC; 2016.
[28] Torres-Rodas P, Fayaz J, Zareian F. Strength resistance factors for seismic design of exposed based plate connections in special steel moment resisting frames. Earthquake Spectra 2020;36(2):537–53. https://doi.org/10.1177/8755293019891714.
[29] Torres-Rodas P, Zareian F, Kanvinde A. Seismic demands in column base connections of steel moment frames. Earthquake Spectra 2018;34(3):1383–403.
[30] Lignos DG, Krawinkler H. A database in support of modeling of component deterioration for collapse prediction of steel frame structures. Struct Eng Res Front 2007. https://doi.org/10.1061/40944(249)31.
[31] Blume J. A Structural Dynamic Analysis of Steel Plant Structures Subjected to the May 1960 Chilean Earthquakes. Bull Seismol Soc Am 1963;53(2):439–80.
[32] Tremblay R, Mitchell D, Tinawi R. Damage to industrial structures due to the 27 February 2010 Chile earthquake. Can J Civ Eng 2013;40(8):735–49. https://doi.org/10.1139/cjce-2012-0197.
[33] Habbit DKB, Sorenson P. ABAQUS Analysis User's Manual Version 6.14-1. Dassault Systems. France 2014.
[34] Gupta A, Krawinkler H. Prediction of Seismic Demands for SMRF's with Ductile Connections and Elements. SAC Joint Venture 2002.
[35] Grigoriev IS, Meilikhov EZ, editors. Handbook of physical quantities. CRC Press; 1996.
[36] Trautner CA, Hutchinson TC. Parametric Finite-Element Modeling for Exposed Steel Moment Frame Column Baseplate Connections Subjected to Lateral Loads. J Struct Eng 2018;144(6):04018049. https://doi.org/10.1061/(asce)st.1943-541x.0001990.
[37] American Concrete Institute. Building Code Requirements for Structural Concrete AC1 318-19. ACI; 2019.
[38] Instituto Nacional de Normalizacion. NCh 2369 Of 2003 Diseño sismico de estructuras e instalaciones industriales. INN; 2003. (in Spanish).
[39] American Institute of Steel Construction. Prequalified connections for special and intermediate steel moment frames for seismic applications ANSI/AISC 358-16. AISC; 2016.
[40] Thapa D, Pantelides CP. Self-Centering Bridge Bent with Stretch Length Anchors as a Tension-Only Hysteretic Hybrid System. J Struct Eng 2021;147(10):4021163.